UC Merced

UC Merced Previously Published Works

Title

Receiver shape optimization for maximizing medium temperature CPC collector efficiency

Permalink

https://escholarship.org/uc/item/4cz8w769

Journal

Solar Energy, 122

Authors

Karwa, Nitin
Jiang, Lun
Winston, Roland

Publication Date

2015-12-01

Peer reviewed

Receiver shape optimization for maximizing medium temperature CPC collector efficiency

Nitin Karwa [a,*], Lun Jiang [b], Roland Winston [b], Gary Rosengarten [a]

[a] *School of Aerospace, Mechanical and Manufacturing Engineering, RMIT University, Melbourne, VIC 3000, Australia*
[b] *Schools of Natural Science and Engineering, University of California at Merced, Merced, CA 95343, USA*

Abstract

Low optical-concentration solar thermal CPC collectors for process heat at 150–300 °C generally use thermal oil as the collector fluid. Thermal oils have low thermal conductivity and high viscosity, which leads to significant thermal resistance and hence reduced collector thermal efficiency. One way to minimize the thermal resistance is by having turbulent flow of the thermal oil within the receiver. For a given receiver area and mass flow rate of the fluid, this can be achieved by narrowing the flow passage but keeping the receiver area constant by adding external flat fins. In this paper a new receiver design for a compound parabolic concentrator is proposed which is a hybrid of a U-shaped tubular receiver and a bifacially irradiated flat receiver. To keep the receiver area constant, the fins are increased in width as the tube diameter is decreased. Its performance when enclosed in a glass vacuum tube and a CPC has been modelled. The transmission and absorption of solar energy, optical losses due to the receiver–reflector gap, heat transfer within the receiver, and the thermal losses have been modelled. Keeping the receiver area and fluid flow rate constant, the thermal resistance of the thermal oil flow within the receiver reduces when the flow passage is narrowed leading to increased thermal efficiency. On the other hand, the hybrid receiver has lower optical efficiency as compared to a tubular receiver due to its higher gap loss. Overall, the hybrid receiver has similar or better thermal efficiency than the tubular receiver. Thermal efficiency and effective thermal efficiency, which accounts for the pumping power penalty, shows that the performance improvement with thermal oil due to receiver shape optimization depends on the receiver area, concentration ratio, absorptivity and emissivity of the selective surface, the mass flow rate through the receiver and fluid temperature. Highest effective thermal efficiency is generally achieved in the laminar–turbulent transitional regime. For temperatures below 150 °C, water has been found to give better performance than thermal oil at all mass flow rates with no significant improvement in collector performance achieved by reducing the tube diameter.
© 2015 Elsevier Ltd. All rights reserved.

1. Introduction

A large fraction of global energy consumption is associated with meeting the thermal requirements for buildings and industrial processes at temperatures up to 400 °C, which can be met using solar energy. For example, solar thermal collectors with output temperatures of 150–250 °C have been integrated with double/triple vapour absorption chillers for building air conditioning by various researchers (Li et al., 2014a; Winston et al., 2014). In order to achieve temperatures above 150 °C, the solar energy needs to be concentrated. The parabolic trough collector, a line focus

---

Nomenclature

A	area, m^2		ρ	absorptance, –
C	ideal concentration ratio, –		σ	Stefan–Boltzmann constant, $W/m^2\,K^4$
C'	geometric concentration ratio, –		τ	transmittance, –
c	specific heat capacity, J/kg K			
d_i	tube inside diameter, m		*Subscripts*	
d_o	tube outside diameter, m		a	aperture
F_{12}	view factor from surface 1–2, –		B	beam
f	friction factor, –		b	fin base
g	gap, m		CPC	compound parabolic concentrator
h	heat transfer coefficient, $W/m^2\,K$		D	diffuse
I	radiation flux, W/m^2		e	enclosure
k	thermal conductivity, W/m K		eff	effective
L	length of flow passage, m		e–∞	enclosure to ambient
l	length of collector, m		f	fluid
l_t	thermal development length, m		fin	fin
$\dot{m}$	mass flux per unit aperture area, $kg/s\,m^2$		g	gap
Nu	Nusselt number, –		i	inner surface
P	power, W		m	mirror
p	perimeter, m		hyd	hydraulic
Pr	Prandtl number, –		t	thermal equivalent
Q	heat transfer rate, W		op	optical
Re	Reynolds number, –		o	outer surface
T	temperature, °C		r	receiver
u	velocity of fluid in the tube, m/s		r–e	receiver to enclosure
w	fin width, m		ref	reference receiver
			sky	sky
Greek symbols			th	thermal
α	reflectance, –		u	utilized
δ	fin thickness, m		V	virtual receiver enclosing the receiver and the gap
ε	emissivity, –			
η	efficiency, –		v	virtual receiver enclosing just the receiver
θ_A	acceptance half-angle of a CPC, radian		wind	wind
v	kinematic viscosity, m^2/s		∞	ambient

design, is the most widely used concentration technology. Low-concentration non-imaging-optics based compound parabolic concentration (CPC) devices, may be cheaper than parabolic trough collectors for achieving temperatures up to 300 °C as they do not require tracking and can also collect a part of the diffuse radiation. However, the concentration of a stationary collector is much lower, which results in lower collector thermal efficiency in high Direct Normal Irradiance (DNI) areas as compared to parabolic trough collectors. In low DNI conditions parabolic troughs are ineffective.

In order to improve collector thermal efficiency at higher temperatures, evacuated tubes are used as they reduce the convective and conductive losses from the absorber. Some CPC solar collectors integrate a Dewar-type evacuated tube, where the solar energy is absorbed by the selective-coated inside glass tube (Li et al., 2014b). The absorbed heat is then conducted by means of press-fitted aluminium

or copper fins to copper tubes through which the working fluid flows. The absorber along with the fins and tubes is called the receiver. Any thermal resistance within the receiver will have a negative effect on the collector thermal performance. O'Gallagher (2008) reported a substantial reduction in the thermal performance of a CPC collector with Dewar-type evacuated tube due to the thermal contact resistance between the inner surface of the absorber tube and the fin. An alternative receiver design for a CPC collector, which is similar to that of a parabolic trough collectors, consists of a selective-coated metallic tube absorber enclosed within an evacuated glass enclosure (Winston et al., 2014). The thermal contact resistance is absent as a result of direct irradiation of the absorber tubes carrying the heat transfer fluid and the maximum thermal resistance in the receiver is due to the fluid. Nkwetta et al. (2013) compared the thermal performance of two partially evacuated tube integrated CPC collectors, one with a directly

irradiated heat pipe receiver and another with a directly irradiated water flow receiver of a tubular shape (counter flow design) at temperatures up to 80 °C. The heat pipe design was reported to have about 37% lower loss coefficient than the direct flow design. This is most likely due to the higher resistance to heat transfer attributed to the water flow in the direct flow design as compared to the near negligible value of resistance in the case of the heat pipe. It is therefore necessary to minimize this thermal resistance in order to achieve a collector efficiency factor as close to one as possible (Duffie and Beckman, 2013).

Various strategies have been adopted in the past to achieve a collector efficiency factor close to one by reducing the receiver thermal resistance in solar collectors. Here we discuss a specific example of a non-evacuated sheet-and-tube solar water heater (Duffie and Beckman, 2013). In this design, the receiver comprises of small diameters tubes with water flowing through them which are then bonded (typically brazed or welded) to the underside of a directly irradiated flat plate absorber. The underside of receiver, comprising of the flat plate and the bonded tubes, is insulated from the ambient. The flat plates act as fins bonded to a tube, conducting the absorbed solar energy in the form of heat to the tubes. Four resistances exist in series between the absorber and the water flowing in the tubes: resistance of the plate, the bond resistance between the plate and the tubes, resistance of the tube wall and the convective resistance of flowing water. These collectors are designed for low water mass flow rate of about 0.02 kg/s per square meter of collector gross area (Australian/New Zealand Standard, 2007). Yeh et al. (2003) showed that reducing the number of tubes reduces the convective resistance. For a fixed tube centre-to-centre spacing and plate thickness, Duffie and Beckman (2013) showed that the thermal performance of these collectors can be improved when the water flow in the tubes is turbulent as compared to laminar. At a fixed water flow rate, two methods can be adopted to reduce the convective thermal resistance. One method is to fix the receiver geometry and incorporate passive devices like twisted tapes, ribbed walls, and fins, to enhance the heat transfer coefficient. Hong and Bergles (1976) showed that the laminar flow heat transfer coefficient can be enhanced a few hundred percent using twisted tape inserts. Jaisankar et al. (2009) showed that twisted tape insert is effective in improving collector thermal performance even in turbulent flow regime when Reynolds number is in the range of 3 000–23 000. Ho and Chen (2008) reported an improvement in thermal performance due to internal fins. The other strategy adopted to reduce the convective thermal resistance is to increase the flow Reynolds number in the tubes. For a fixed mass flow rate this can be either achieved by decreasing the number of tubes (Yeh et al., 2003) or reducing the tube diameter. Yeh et al. (2003) reported that reducing the number of tubes but keeping the tube centre-to-centre spacing and collector area constant (which means that collector width is reduced and the length is correspondingly increased),

leads to only slight improvement in collector thermal efficiency but at the expense of increased pumping losses. Robles et al. (2014) have recently showed that minichannel (hydraulic diameter of 1.42 mm) receivers give better thermal efficiency than sheet-and-tube receivers in non-evacuated flat plate solar water heater systems but they did not discuss the additional pumping power requirements of these minichannel collectors. Depending on the mass flow rate and the solar intensity, an optimum tube diameter and spacing must exist where the resource utilization efficiency is maximum.

Low optical-concentration solar thermal collectors employed for heat at 200–400 °C generally use thermal oil as the collector fluid, for example in the study of Winston et al. (2014). Thermal oils have lower thermal conductivity and higher viscosity than water and the resulting thermal resistance of the flow may be much more significant than in flat plate solar water heaters. To reduce the thermal resistance for a large absorber, Kim et al. (2013) designed a CPC collector with a cylindrical absorber that was constructed by solar selective coated copper sheet (2 mm thick) formed into cylindrical shaped and a metallic counter flow tube was welded on its inside. Adding a large fin to the counter flow tube instead of a single bare tube of larger diameter resulted in a high oil flow velocity within the tubes and lower convective thermal resistance. They showed that the thermal performance of a CPC thermal collector operating at high temperatures of up to 250 °C improves with the increase in oil mass flow rate through the tube. Similar findings were reported by Balkoski (2011) for a cylindrical receiver but with a U-tube instead of a counter flow tube. The improvement in collector performance with increase in mass flow rate was due to the reduction in fluid thermal resistance, which suggests that the tube and the fin dimensions should be optimized based on mass flow rate through the collector. Another important consideration in selecting the tube dimension is its effect on the pumping power requirement as it significantly increases with increased fluid velocity. Oils have higher viscosity and lower heat capacity as compared to water, which increases the pumping power as compared to water as the working fluid. However, Kim et al. (2013) did not report the variation of the pumping power with increasing mass flow rate. Sharma and Diaz (2011) showed that a CPC collector with minichannel (3 mm diameter) receiver has superior thermal performance than a receiver with large flow passages but pumping losses were not compared. Besides the tube diameter, the fin thickness must also be optimized as its thermal resistance might be significant in large receivers. A thorough analysis of collector performance must include both the thermal and hydraulic performance to optimize the collector dimensions. The present study reports results of performance modelling of CPC solar collectors and the effect of receiver geometry on the thermo-hydraulic performance of the collector.

The receiver design evaluated in this study is a hybrid of a U-tube receiver and a bifacial flat receiver. The receiver is

enclosed in an evacuated tube and mounted in a CPC. The optical performance, useful heat gain in the collector and pumping losses are modelled. Across all the hybrid receiver designs, the receiver area is kept constant while the tube diameter and the widths of the fins are varied, with an objective to optimize the shape of the receiver to achieve the highest thermohydraulic performance.

2. Receiver geometry

In the present study, the design consist of a directly irradiated solar selective coated metallic receiver enclosed in a glass evacuated tube (enclosure), which is placed in an uncovered CPC as shown in Fig. 1. Two types of receivers are studied and their shapes are shown in the inset. The reference design, shown in Fig. 1a, is a hairpin design, where a circular tube is arranged in a U-shape with negligibly small gap between the two legs of the hairpin. This small gap between the two legs results in zero lateral heat conduction between the two legs. The net radiation exchange between the two legs is expected to be negligible as the surfaces have low emissivity and their temperatures are very close to each other. A close return bend is used to construct the 180 degree turn. Typical close return bends have a bend radius equal to the tube diameter, so a reducer coupling is necessary. The other receiver design, shown in Fig. 1b, is a hybrid of a U-tube receiver (which is called the reference

receiver in this study) and a bi-facially radiated flat receiver. In this paper, the flat portion of the receiver will be referred to as the fin. The whole surface of the receiver is assumed to be uniformly irradiated by solar radiation entering the aperture of the CPC. The heat transfer fluid flows through the tube and is heated by the radiation absorbed at the surface of the receiver.

Consider the hybrid receiver configuration shown in Fig. 1b. The U-shaped receiver has two legs (called the incoming and outgoing legs in the figure), each of length l. Each leg consists of a tube of inside diameter d_i and outside diameter d_o (see Fig. 2). Integral fins, each of length w and thickness δ, on either side of the tube complete the receiver. The working fluid flows through the tube. Both the fin and the tube are irradiated by solar radiation and the absorbed solar radiation minus the thermal losses is transferred to the working fluid by conduction though the fin and the tube wall, and then by convection in the fluid. The reference receiver is a special case of the hybrid receiver where the fin width is zero. Ignoring the 180 degree U-bend length, the total length of the receiver and the fluid flow path length are l and $2l$, respectively. The total perimeter of the receiver is given by

$$p_r = 2(\pi d_o + 4w). \qquad (1)$$

The perimeter of each leg of the receiver is $p_r/2$. The surface area of the receiver is given by
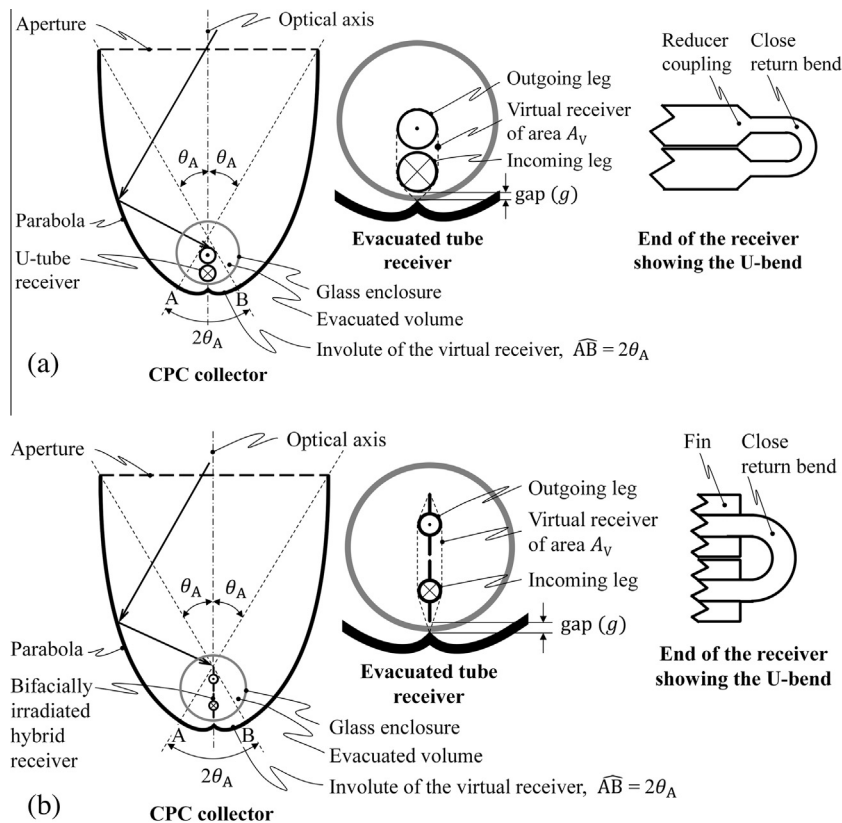

Fig. 1. Cross-section of a CPC designed for (a) a U-tube receiver without fins, and (b) a hybrid of bifacially irradiated flat receiver and a U-tube receiver. The CPC is to be designed for a virtual receiver shown by dotted lines in the inset of both the figures. The U-bend is also shown on the right end of each figure. Depending upon the size of the tubes and their centre-to-centre spacing, a reducer coupling might be necessary to accommodate a close return bend.
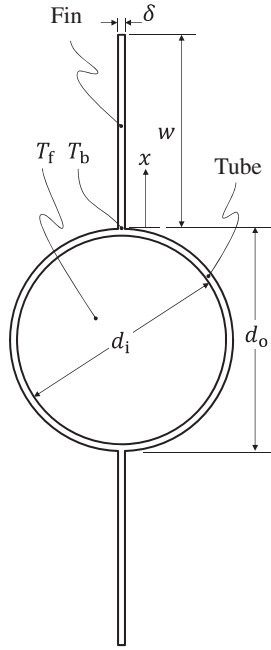
Fig. 2. A schematic showing the receiver leg along with its dimensions. Both the fin and the tube are made of the same metal, which is copper in this study.

$$A_r = p_r l. \tag{2}$$

For a truly ideal CPC, the CPC reflector must touch the receiver. In practise, the presence of the glass enclosure around the receiver results in a narrow gap between the receiver and the CPC. Additionally, the receiver must not touch the enclosure, which further adds to the receiver reflector gap. This results in a part of the reflected solar radiation passing through the gap and missing the receiver. This loss, called the gap loss, depends on the receiver shape (O'Gallagher, 2008) and is determined analytically in the present study. Furthermore, the two receivers that are being investigated in the study have concave sections. Accounting for the gap and the concave shape, the CPC is to be designed for a virtual receiver shown in the insets in Fig. 1 by dotted segments using the "extended cusp gap solution" (Winston, 1978).

3. Mathematical modelling of the thermal processes

The mathematical model is subdivided into five sections: (a) the absorption of solar radiation in the receiver and the enclosure, (b) thermohydraulics of the receiver, (c) thermal losses from the receiver and enclosure, (d) energy balance, and (e) performance evaluation criterion. The following assumptions are made for the theoretical analysis.

1. The CPC is full, ideal and designed for a virtual receiver enclosing the receiver and the gap (shown in Fig. 1) using the extended cusp gap method and the acceptance half-angle is given by

$$\theta_A = \arcsin(A_V/A_a), \tag{3}$$

where A_V is the surface area of the virtual receiver enclosing the absorber and the gap, and A_a is the aperture area. The ideal geometric concentration ratio is given by

$$C = 1/\sin\theta_A. \tag{4}$$

A geometric concentration ratio can be defined based on the receiver and aperture areas as

$$C' = A_a/A_r. \tag{5}$$

2. Any beam radiation incident on the aperture within the acceptance angle will be reflected by the mirrors of the CPC on to the receiver and the gap. On the other hand, the fraction of diffuse radiation entering the aperture that will reach the receiver is given by the view factor from the aperture to the receiver (Rabl et al., 1979).

To determine the gap loss fraction, the flux distribution on the virtual receiver is assumed to be diffuse, as suggested by Rabl et al. (1979). This gives a good estimate of the average gap loss over the full range of incidence angle up to the acceptance angle. Also an additional virtual receiver which encloses just the receiver is defined and its area is A_v. As the virtual receiver "v" enclosing just the receiver has no concave sections and is completely surrounded by the virtual receiver "V" enclosing the receiver and the gap, all the radiation leaving it will strike the virtual receiver "V", that is $F_{vV} = 1$. Applying the reciprocity relation $A_V F_{Vv} = A_v F_{vV}$ gives $F_{Vv} = A_v/A_V$. Also the view factor from the virtual receiver "v" to the receiver $F_{vr} = 1$. As the entire beam radiation incident on the aperture will reach the virtual receiver "V", the fraction of this radiation that will reach the receiver is given as

$$F_r = 1 - F_g = F_{Vv} \times F_{vr} = A_v/A_V, \tag{6}$$

where F_g is the gap loss fraction. O'Gallagher (2008) also recommends a similar approach to calculate the gap loss. The virtual receiver areas are given by

$$A_V = \left\{ 2\sqrt{w^2 + wd_o} + 2\sqrt{(w+g)^2 + (w+g)d_o} + 4w \right.$$
$$+ d_o \left[2 + \pi - \arccos\left(\frac{d_o}{d_o + 2w}\right) \right.$$
$$\left. - \arccos\left(\frac{d_o}{d_o + 2w + 2g}\right) \right] \left. \right\} l \tag{7}$$

and

$$A_v = \left\{ 4\sqrt{w^2 + wd_o} + 4w \right.$$
$$+ d_o \left[2 + \pi - 2\arccos\left(\frac{d_o}{d_o + 2w}\right) \right] \left. \right\} l. \tag{8}$$

The derivations of Eqs. (7) and (8) are given in Appendix B. Fig. 3 shows the variation of F_g with the ratio of tube perimeter to the receiver perimeter for the hybrid receiver. A non-monotonous dependence can be seen, with the lowest gap loss occurring when fins are absent,
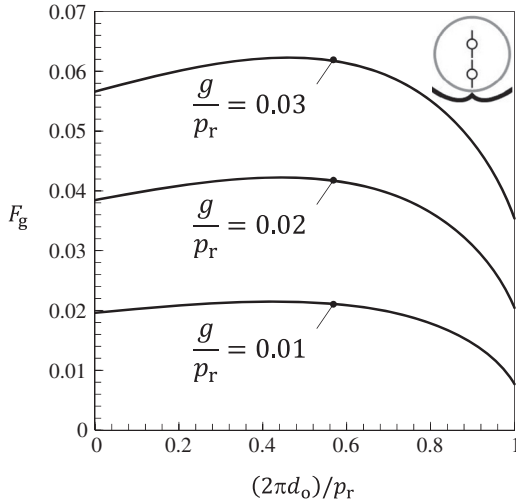
Fig. 3. Variation of the gap loss fraction with the geometric proportions of the receiver (ratio of the tube perimeter to the receiver perimeter) for different gap width to perimeter ratios.

i.e. the reference receiver. This non-monotonous relationship between the two further leads to a non-monotonous dependence of optical efficiency with the tube diameter. For the same gap size, the increase in gap loss with the decrease in tube diameter becomes more significant as the receiver perimeter reduces.

3. Any beam radiation entering the aperture is subjected to multiple reflections before reaching the enclosure. To determine the effective incidence angle of the rays on any surface (mirror, enclosure and receiver) will require detailed ray tracing simulation, which is out of the scope of the present study. Therefore, the optical properties of the mirror and the receiver are assumed to be independent of the incidence angle. The optical properties of the enclosure have been obtained from a previous study by the present researchers (Gajic et al., 2014).

4. Temperature difference between the outside and the inside surfaces of the glass enclosure is calculated to be always less than 1 K for the range of parameters investigated and therefore the thermal resistance of the enclosure is neglected in the model.

5. Thermal losses from the end of the collector have not been considered in the analysis.

6. The end effects due to finite length of the absorber and non-normal angle of incidence in the longitudinal plane has not been considered in the analysis.

3.1. Absorption of solar radiation

With the above assumptions, solar radiation absorbed by the enclosure and the receiver can be formulated. The variation of the average number of times any beam/diffused radiation gets reflected by the CPC walls before reaching the enclosure and thereafter the receiver is given by Rabl et al. (1979) as

$$N = 1 + 0.07C. \tag{9}$$

The optical transmission of the CPC accounts for reflection losses and is a function of the average number of reflections (Rabl et al., 1979). For both beam and diffuse radiation, neglecting the end effects of the CPC, the optical transmission of the CPC is given by

$$\tau_{CPC} = \bar{\tau}_{CPC} = \rho_m^N. \tag{10}$$

The overline (macron) indicates that the surface properties for incident diffuse radiation.

The total solar radiation energy incident on the aperture is given by

$$Q_a = (I_B + I_D)A_a, \tag{11}$$

where A_a is the aperture area. The enclosure absorbs a part of the beam solar radiation, which is given by

$$Q_{e,B} = I_B A_a \tau_{CPC}(\alpha_e + \tau_e \rho_r F_{re} \bar{\alpha}_e). \tag{12}$$

The second term in Eq. (12) is the fraction of incident energy on the receiver that is reflected back and then absorbed by the enclosure. The reflected radiation from the receiver is diffuse, so the absorptance of the enclosure for diffuse radiation $\bar{\alpha}_e$ has been used. Here F_{re} is the view factor from the receiver to the enclosure. As the glass enclosure has high transmittance to the solar radiation and the receiver has high absorptance for solar radiation, higher order terms become extremely small and thus are not included in the model. Assuming the diffuse radiation entering the aperture is distributed isotropically by the mirrors, the fraction of radiation incidence on the aperture that reaches the enclosure and the receiver is given by the view factors from the aperture to the these surfaces. The diffuse part of the radiation that gets absorbed by the enclosure is

$$Q_{e,D} = I_D A_a \bar{\tau}_{CPC}(F_{ae}\bar{\alpha}_e + F_{ar}\bar{\tau}_e\bar{\rho}_r F_{re}\bar{\alpha}_e). \tag{13}$$

F_{ae} and F_{ar} are the view factors from the aperture to the enclosure and to the receiver, respectively. The total solar radiation energy absorbed by the enclosure is given by

$$Q_e = Q_{e,B} + Q_{e,D}. \tag{14}$$

The solar energy absorbed by the receiver is given by

$$Q_r = Q_{r,B} + Q_{r,D}, \tag{15}$$

which are given by

$$Q_{r,B} = I_B A_a \tau_{CPC}\tau_e F_r(\alpha_r + \rho_r F_{re}\bar{\rho}_e F_{er}\bar{\alpha}_r), \tag{16}$$

and

$$Q_{r,D} = I_D A_a \bar{\tau}_{CPC}\bar{\tau}_e F_{ar}(\bar{\alpha}_r + \bar{\rho}_r F_{re}\bar{\rho}_e F_{er}\bar{\alpha}_r). \tag{17}$$

Here F_{er} is the view factor from the enclosure to the receiver. All the view factors are summarized in Appendix A.

3.2. Thermohydraulic performance of the receiver

The assumptions made for deriving the expression for heat transfer within the receiver are:

1. The solar flux distribution is uniform on the receiver. This assumption gives a good estimate of the temperature distribution in the fin over the full range of incidence angle up to the acceptance angle.
2. Lateral heat exchange between the receiver legs is negligible.
3. The thermal losses from the fin and the tube are by radiation. Instead of determining them locally over each element of the receiver, it is determined by assuming the receiver at an average temperature.
4. The fin is thin and of high thermal conductivity, so the temperature gradient though the fin thickness is negligible. Also, the thermal resistance of the solar selective coating is negligible. Additionally, the solution is determined for the mean fluid temperature and the temperature gradient in the fin in the direction of fluid flow is not considered. The temperature gradients within the tube wall and its thermal resistance are negligible. These assumptions were confirmed by an ANSYS simulation.

The fin shown in Fig. 4 is of length l in the fluid flow direction. The free end tip of the fin is treated as insulated, while the end attached to the tube is at a temperature T_b. Uniform energy flux of intensity I is applied of the other two faces. In the case of the solar receiver, this intensity I is the difference of absorbed solar radiation flux and the thermal loss flux. As the thermal losses from the receiver are only by thermal radiation, the expected small gradient (less than 10 K) in fin temperature from base to tip will results in a very small variation in the loss coefficient along the fin width, which has been assumed to be negligible. Combining this assumption with the assumption of

uniform solar flux distribution, the intensity I is taken to be uniform across the fin width. The energy balance for an elemental region of width Δx is shown in the inset of Fig. 4 and can be written as

$$-k_r A_{\text{fin}} \frac{dT}{dx}\bigg|_x = -k_r A_{\text{fin}} \frac{dT}{dx}\bigg|_{x+\Delta x} + I p_{\text{fin}} \Delta x, \tag{18}$$

where $A_{\text{fin}} = l\delta$ is the cross-section of the fin in the direction of heat flow (i.e. towards the tube) and $p_{\text{fin}} = 2(l + \delta)$ is its perimeter, as also shown in the schematic of the fin. δ is the fin thickness and k_r is the thermal conductivity of receiver material. In the limit, as Δx approaches zero

$$k_r A_{\text{fin}} \frac{d}{dx}\left(\frac{dT}{dx}\right) = -I p_{\text{fin}}. \tag{19}$$

Since $\delta \ll l$, $p_{\text{fin}}/A_{\text{fin}} = 2/\delta$. The temperature profile along the width of the fin has to satisfy the following boundary conditions at its base ($x = 0$) and at its tip ($x = w$)

$$T|_{x=0} = T_b, \tag{20}$$

$$\frac{dT}{dx}\bigg|_{x=w} = 0. \tag{21}$$

Integration of Eq. (19) twice with respect to x and applying the above boundary conditions gives

$$T_x = T_b + \frac{I}{k_r}\left(\frac{2wx}{\delta} - \frac{x^2}{\delta}\right). \tag{22}$$

The mean fin temperature is calculated as suggested by Bliss Jr (1959)

$$T_{\text{fin}} = \int_0^w (T_x dx)/w = T_b + \frac{2}{3}\frac{I}{k_r}\frac{w^2}{\delta}. \tag{23}$$

The intensity I can be written as

$$I = \frac{Q_u}{p_r l}. \tag{24}$$

Q_u is the useful heat gained by the fluid from the absorber as it flows from the inlet to the outlet of the receiver. Substituting I in the form of Q_u in Eq. (24) gives

$$T_{\text{fin}} = T_b + \frac{2}{3}\frac{Q_u}{p_r l}\frac{1}{k_r}\frac{w^2}{\delta}. \tag{25}$$

The thermal resistance of the tube wall is negligibly small and Q_u, from heat transfer consideration, is given by

$$Q_u = h_f(2\pi d_i l)(T_b - T_f), \tag{26}$$

where h_f is the convective heat transfer coefficient on the inside of the tube. Rearranging the above equation gives

$$T_b = T_f + \frac{Q_u}{h_f(2\pi d_i l)}. \tag{27}$$

Substituting T_b from the above equation into Eq. (25) gives

$$T_{\text{fin}} = T_f + \frac{Q_u}{h_f(2\pi d_i l)} + \frac{2}{3}\frac{Q_u}{p_r l}\frac{1}{k_r}\frac{w^2}{\delta}. \tag{28}$$
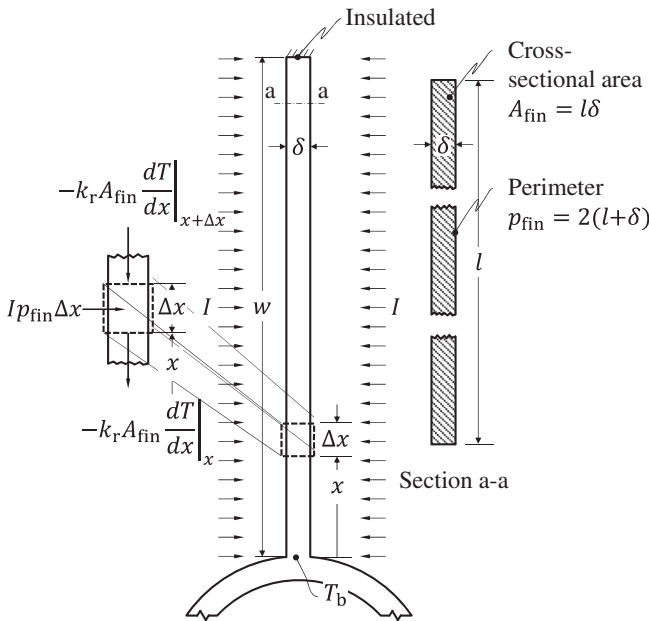

Fig. 4. A schematic representation of heat transfer within the fin. The heat transfer has been assumed to be one dimensional along the direction x by ignoring temperature gradients across the thickness of the fin.

The area-weighted average temperature of the receiver is given by

$$T_r = \frac{T_b(\pi d_o) + T_{fin}(4w)}{p_r/2}. \tag{29}$$

The thermal loss can be calculated at T_r. Substituting T_b and T_{fin} from Eqs. (27) and (28), respectively and rearranging the above equation results in a direct expressions for Q_u in the form of T_r and T_f.

$$Q_u = \frac{(T_r - T_f)A_r}{\frac{1}{h_f}\left(\frac{d_o}{d_i} + \frac{4w}{\pi d_i}\right) + \frac{16}{3}\frac{1}{p_r}\frac{1}{k_r}\frac{w^3}{\delta}}. \tag{30}$$

Therminol 66, a widely used solar collector working fluid for temperatures up to 345 °C, is the working fluid in the present study. Thermal properties of Therminol 66 as a function of temperature were obtained from Solutia Inc. (2001). The thermal conductivity of thermal oils is almost 1/6th of water. The Prandtl number is about 58 at 100 °C and monotonously decreases with increasing temperature to a value of about 10 at 340 °C. Due to its high Prandtl number, depending on the flow Reynolds number, the thermal development length of thermal oils may be comparable or greater than the collector length for laminar flow as shown in Fig. 5, and it has to be taken into account in the heat transfer coefficient calculation. Pumping losses have to be calculated to determine the net performance of the collector.

The Reynolds number for the flow within the tube is defined as

$$Re = \frac{u_f d_i}{v_f}, \tag{31}$$

where u_f is the flow velocity and v_f is the kinematic viscosity of the fluid. The velocity can be written in the form of collector mass flux ($\dot{m}_f$) as

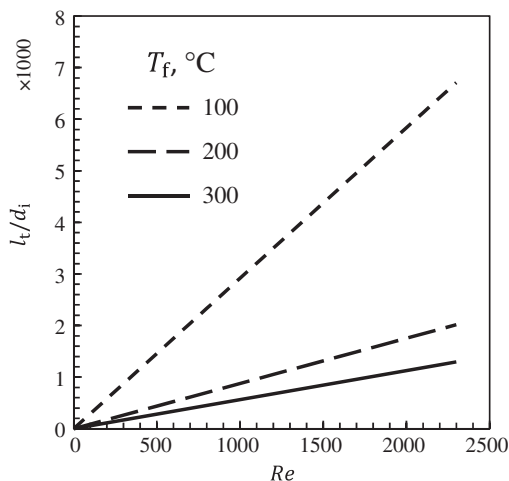$$u_f = \frac{\dot{m}_f A_a}{\rho_f}\left(\frac{4}{\pi d_i^2}\right). \tag{32}$$

Fig. 5. Development length for a laminar flow of Therminol 66.

The heat transfer coefficient is determined from Nusselt number correlations. The Nusselt number is defined as

$$Nu = \frac{h_f d_i}{k_f}. \tag{33}$$

The Nusselt number for all the regimes can be estimated from the correlation of Gnielinski (2010). For laminar flow ($Re < 2300$) with a constant heat flux boundary condition and simultaneously developing thermal and hydrodynamics boundary layers, the Nusselt number given by

$$Nu = \left\{4.364^3 + 0.6^3 + \left[1.953(Re\,Pr\,d_i/L)^{1/3} - 0.6\right]^3 \right.$$
$$\left. + \left[0.924(Re\,d_i/L)^{1/2}Pr^{1/3}\right]^3\right\}^{1/3}, \tag{34}$$

Here L is the length of the flow passage. This correlation is valid for $0 \leq d_i/L \leq 1$ and $Pr \geq 0.6$. The Darcy friction factor for laminar flow ($Re < 2300$) is

$$f = 64/Re. \tag{35}$$

For the turbulent flow regimes ($Re \geq 10^4$), Nusselt number is given by

$$Nu = \frac{(f/8)Re\,Pr}{1 + 12.7\sqrt{f/8}(Pr^{2/3} - 1)}\left\{1 + \left(\frac{d_i}{L}\right)^{2/3}\right\}, \tag{36}$$

where

$$f = \left(1.8\log\frac{Re}{6.8}\right)^{-2}. \tag{37}$$

For calculation of heat transfer coefficient in the transition regime ($2300 < Re < 10^4$), the following linear interpolation is suggested by Gnielinski (2010).

$$Nu = (1 - \alpha)\,Nu_{Re=2300} + \alpha Nu_{Re=10^4}, \tag{38}$$

with

$$\alpha = \frac{Re - 2300}{10^4 - 2300}. \tag{39}$$

$Nu_{Re=2300}$ is calculated at $Re = 2300$ using Eqs. (34) while $Nu_{Re=10^4}$ is calculated at $Re = 10^4$ using Eqs. (36) and (37). This correlation is valid for $0.6 \leq Pr \leq 1000$ and $0 \leq d_i/L \leq 1$. The length of the flow passage in the collector is $L = 2l$. Cheng (2008) suggested the following interpolation function for the friction factor in the transition regime ($2300 < Re < 10^4$)

$$f = \left(\frac{64}{Re}\right)^\beta\left(1.8\log\frac{Re}{6.8}\right)^{2(\beta-1)}, \tag{40}$$

with

$$\beta = \frac{1}{1 + (Re/2720)^9}. \tag{41}$$

The pressure drop in a closed return bend is calculated using the 3-K method (Hall, 2012). The hydraulic power to pump the fluid through the collector is given by

$$P_{\text{hyd}} = \left(f \frac{2l}{d_{\text{i}}} + K \right) \frac{\rho_{\text{f}} u^2}{2} \frac{\dot{m}_{\text{f}} A_{\text{a}}}{\rho_{\text{f}}}. \tag{42}$$

$\dot{m}_{\text{f}}$ is the mass flow rate through the collector per unit aperture area. The resistance coefficient K for the closed return bend (Hall, 2012) is given by

$$K = \frac{1000}{Re} + 0.12 \left(1 + \frac{1.329}{d_{\text{i}}^{0.3}} \right). \tag{43}$$

All the thermal properties are calculated at the mean fluid temperature given by $T_{\text{film}} = (T_{\text{f}} + T_{\text{b}})/2$.

Since a thermal energy source, such as a carbonaceous fuel, is used in power stations to produce the needed electrical power, the thermal equivalent of the pumping power is calculated by taking the thermo-electric conversion process efficiency referred to the consumer point. The world average efficiency of electricity production from all fossil fuels in public electricity and CHP plants was 36% between year 2001 and 2005 (Trudeau and Francoeur, 2008). Average electricity transmission and distribution efficiency in the US in 2013 was 91.2% (US Energy Information Administration, 2015). The transmission and distribution efficiency data is unavailable for the whole world, so the data from United States is used. Combining these efficiencies, the overall efficiency for electricity generation, transmission and distribution (η_{GTD}) is taken as 33%, which was also used by Karwa et al. (2001). The thermal equivalent of the mechanical pumping power is given by

$$P_{\text{t}} = \frac{P_{\text{hyd}}}{\eta_{\text{pump}} \eta_{\text{GTD}}}. \tag{44}$$

In the present study, the pump efficiency η_{pump} is taken to be 80%. The power lost in overcoming frictional resistance is also converted into heat, so the total thermal energy gain of the fluid is given as

$$Q_{\text{total}} = Q_{\text{u}} + P_{\text{hyd}}. \tag{45}$$

If a thermodynamic system is defined including the power station, the transmission system and the pump and the solar collector, then from the first law of thermodynamics, the total energy resource used for achieving a heat gain of Q_{total} is given by

$$P_{\text{total}} = Q_{\text{a}} + P_{\text{t}}. \tag{46}$$

3.3. Thermal losses

The analysis of thermal energy exchange between the receiver and the enclosure, and between the enclosure and the atmosphere/sky gives the thermal losses from the receiver. The thermal energy exchange between the receiver and the enclosure is by diffuse radiation as the vacuum around the receiver completely eliminates conduction and convection heat transfer. The thermal exchange between the enclosure and the atmosphere is by convection, while thermal exchange with the sky is by diffuse radiation. Back

and end losses in the collector are neglected as they have been shown to be negligible by Hsieh (1981).

The receiver emits radiation in the mid and long-wavelength infrared band, while the emission from the glass enclosure is the long and far-wavelength infrared band. The emissivity of TiNOx is spectral dependent even in these spectral bands, while the spectral properties of glass are nearly constant in these spectral bands. The radiation exchange between two selective bodies is given as

$$Q_{\text{r}-\text{e}} = \frac{\sigma(T_{\text{r}} + 273)^4}{\left(\frac{1-\bar{\varepsilon}_{\text{r}}'}{A_{\text{r}}\bar{\varepsilon}_{\text{r}}'} + \frac{1}{A_{\text{r}}F_{\text{re}}} + \frac{1-\bar{\alpha}_{\text{e}}'}{A_{\text{e,i}}\bar{\alpha}_{\text{e}}'} \right)} - \frac{\sigma(T_{\text{e}} + 273)^4}{\left(\frac{1-\bar{\alpha}_{\text{r}}''}{A_{\text{r}}\bar{\alpha}_{\text{r}}''} + \frac{1}{A_{\text{r}}F_{\text{re}}} + \frac{1-\bar{\varepsilon}_{\text{e}}''}{A_{\text{e,i}}\bar{\varepsilon}_{\text{e}}''} \right)}. \tag{47}$$

The superscript ($'$) and ($''$) indicates that the radiation is emitted by the receiver and the enclosure, respectively. $A_{\text{e,i}}$ is the inner surface area of the enclosure which is given as

$$A_{\text{e,i}} = \pi d_{\text{e,i}} l, \tag{48}$$

where $d_{\text{e,i}}$ is the inner diameter of the enclosure. The enclosure loses heat to the surrounding by convection and radiation, which is given by

$$Q_{\text{e}-\infty} = h_{\text{wind}} A_{\text{e,o}} (T_{\text{e}} - T_{\infty})$$
$$+ \sigma \bar{\varepsilon}_{\text{e}}'' A_{\text{e,o}} \left[(T_{\text{e}} + 273)^4 - (T_{\text{sky}} + 273)^4 \right]. \tag{49}$$

$A_{\text{e,o}}$ is the outer surface area of the enclosure which is given as

$$A_{\text{e,o}} = \pi d_{\text{e,o}} l. \tag{50}$$

where $d_{\text{e,o}}$ is the outer diameter of the enclosure. h_{wind} is the wind heat transfer coefficient. It is a function of the wind velocity over the evacuated tube inside the CPC, which depends on the free-stream wind velocity, collector orientation and dimensions of the CPC. Specific correlation for the wind heat transfer coefficient for a glass inside a CPC is unavailable, so we assume a value of 10 W/m² K. Sky temperature T_{sky} is calculated from (Hsieh, 1981)

$$T_{\text{sky}} = T_{\infty} - 6. \tag{51}$$

The model approximates the enclosure to be a small convex grey body exchanging radiation with a large sky, and resultantly the view factor from the sky to the receiver is almost zero.

3.4. Energy balance

The equations derived for solar energy absorption and thermal losses can be used to write steady state energy balance equations for the receiver and the enclosure, respectively, as

$$Q_{\text{r}} - Q_{\text{u}} - Q_{\text{r}-\text{e}} = 0, \tag{52}$$
$$Q_{\text{e}} + Q_{\text{r}-\text{e}} - Q_{\text{e}-\infty} = 0. \tag{53}$$

These two equations are a set of simultaneous non-linear equations which are solved to obtain T_{r} and T_{e}.

A collector performance model was developed in Visual Basic for Applications (VBA) and implanted in MS Excel. These equations were solved using the Solver add-in. The constraints were given by Eqs. (52) and (53), and the solution residuals are typically of the order of 10^{-8}, when converged. The solution was iterated using temperature dependent thermophysical properties till the receiver temperature converged within 0.1%.

3.5. Performance parameters

The optical efficiency is defined as the ratio of solar energy getting absorbed on the receiver surface to the solar energy incident on the aperture, and is given by

$$\eta_{op} = \frac{Q_r}{Q_a}. \tag{54}$$

The optical efficiency in this case also includes the gap loss. The thermal efficiency of the collector is given by

$$\eta_{th} = \frac{Q_u}{Q_a}. \tag{55}$$

Based on the total thermal energy gain in the collector and the total energy resources used in order to achieve this thermal energy gain, an effective thermal efficiency can be defined as

$$\eta_{eff} = \frac{Q_{total}}{P_{total}} = \frac{Q_u + P_{hyd}}{Q_a + P_t}. \tag{56}$$

4. Radiation properties of collector materials

4.1. Mirrors

The mirrors are assumed to be specular. In this study, we assume the reflectance to be independent of the incidence angle. Widely used mirrors in CPC collectors have a reflectance in the range of 0.9 and 0.95. A reflectance value of 0.95 has been chosen for the present study.

4.2. Solar selective coatings

TiNOX is a widely used solar selective coating. Its absorptance of solar radiation, based spectral absorptance for a monochromatic beam incident at 10° to normal, is in the range of 0.944 (Institut für Solartechnik, 2013) to 0.951 (Institut für Solartechnik, 2009). Details of the incidence angle dependence of absorptance are unavailable. We expect the average incidence angle to be more than 10° to normal as beams are reflected multiple times in a CPC before reaching the receiver. It would also depend on the receiver shape. Optical simulations done by the present authors (Gajic et al., 2015) for a CPC with cylindrical receiver showed that the average incidence angle is about 33°.

The emission from TiNOX is diffuse but the spectral absorptance data for 10° incidence angle has been used to report emissivity value of 0.037 at 100 °C (Institut für

Solartechnik, 2013). Values for higher temperature are not available. Using their spectral data, the calculated emissivity at 200 °C is 0.045. However, Surface Optics Corporation (San Diego) experimentally determined the emissivity of a commercial TiNOX foil sample to be 0.158 at 200 °C (Winston, 2012). Their reflectance measurements are spectrally taken from 1.5 μm to 26 μm for normal and near normal incident angles. Additionally, in our measurements with a flat copper sheet receiver with TiNOX coating on the sun exposed face and a highly polished shaded face enclosed in an evacuated tube stagnated at 240 °C when exposed to global tilted radiation of 847 W/m^2 (20% diffuse radiation). Using the above presented mathematical model, the emissivity of TiNOX was calculated at 240 °C to be 0.11. The large difference in emissivity predicted using manufacturer provided hemispherical spectral reflectance measurements, experiments at Surface Optics Corporation (San Diego) and our stagnation tests is likely due to diffuse nature of emitted radiation from TiNOX, which has not been accounted for in the spectrophotometer reflectance measurements. Oxidation of solar selective coatings during the collector manufacturing at high temperature also cannot be ruled out. Due to the uncertainty in TiNOX emissivity value, performance analysis has been done over a range of emissivity values.

4.3. Enclosure

Gajic et al. (2015) simulated the reflection losses from a cylindrical glass tube enclosure (nonabsorbing to solar radiation and wavelength dependent refractive index between 1.48 and 1.55) in a CPC designed for a circular receiver. They determined that for beam radiation incident on the aperture, the average incidence angle of beams reaching the enclosure is around 33°. It remains fairly constant at around this value as the sun rays incidence angle on the aperture increases, before steeply rising as the maximum acceptance angle is reached. Except close to edge ray, the glass tube reflectance was fairly constant at around 12%.

No experimental or simulation results is available for the reflectance of a cylindrical glass tube when exposed to diffuse radiation incident on the CPC aperture. For a flat plate solar collector application, the equivalent incident angle for solar diffuse radiation for various conditions is shown to be 60° (Duffie and Beckman, 2013). The same has been assumed to be true for the cylindrical evacuated tube in a CPC to calculate $\bar{\rho}_e$ using the Fresnel equations assuming the glass to nonabsorbing to the solar radiation.

The radiation emitted by the receiver is diffuse. Similar to that for diffuse solar radiation, for the diffuse thermal radiation emitted by the receiver the equivalent incident angle is assumed to be 60°. The enclosure glass wall thickness is typically between 1.5 and 3 mm. The spectral transmittance of a 2 mm thick borosilicate glass (Borofloat 33) for normal incidence (SCHOTT Technical Glass Solutions GmbH, 2009) is order of 1% for medium to long wave infrared

Table 1
Radiation properties of the enclosure and the receiver.

Enclosure	Receiver
$\rho_e = 0.12$	$\rho_r = 0.056$
$\alpha_e = 0.02$	$\alpha_r = 0.944$
$\tau_e = 0.86$	$\tau_r = 0$
$\bar{\rho}_e = 0.14$	$\bar{\rho}_r = 0.056$
$\bar{\alpha}_e = 0.02$	$\bar{\alpha}_r = 0.944$
$\bar{\tau}_e = 0.84$	$\bar{\tau}_r = 0$
$\bar{\rho}'_e = 0.085$	$\bar{\rho}'_r = 1 - \bar{\varepsilon}'_r$
$\bar{\alpha}'_e = 0.915$	$0.05 \leqslant \bar{\varepsilon}'_r = \bar{\alpha}'_r \leqslant 0.1$
$\tau'_e = 0$	$\bar{\tau}'_r = 0$
$\bar{\varepsilon}''_e = 0.915$	$\bar{\alpha}''_e = 0.03$
$\bar{\rho}''_e = 0.085$	$\bar{\rho}''_r = 0.97$
$\bar{\tau}''_e = 0$	$\bar{\tau}''_r = 0$

The superscript ($'$) and ($''$) indicates that the radiation is emitted by the receiver and the enclosure, respectively. The overline (macron) indicates that the radiation properties for incident/emitted diffuse radiation.

Table 2
Common receiver and enclosure dimensions for the analyzed collectors.

Receiver material	Copper
Receiver thermal conductivity, k_r	400 W/(m K)
Receiver tube wall thickness, $(d_o - d_i)/2$	1 mm
Enclosure wall thickness, $(d_{e,o} - d_{e,i})/2$	2 mm
Gap (=receiver–enclosure gap + enclosure thickness), g	3 mm
Enclosure outer diameter, $d_{e,o}$	$= p_r/2 + 2g$
Collector length, l	1.6 m

radiation. The radiation emitted by the receiver (mid to long wave infrared bands) will be only reflected by the inner surface of the glass enclosure as it does not reach the other face of the enclosure. The reflectance of the enclosure diffuse radiation emitted by the receiver is calculated using the Fresnel equations assuming the glass to fully absorbing to medium and long wave infrared radiation. The refractive index for Borofloat 33 is not available for mid to long wave infrared bands and therefore the refractive index for solar radiation (about 1.47) has been used here.

The radiation properties of the enclosure and the receiver are summarized in Table 1.

5. Results and discussion

The analysis has been done for a wide range of parameters such as CPC's geometric concentration ratio, geometric shape and perimeter of the receiver, emissivity of the receiver, and fluid mean temperature and collector mass flux. Some of the dimensions and materials common to all the analyzed collectors are listed in Table 2.

The working fluid in a solar field runs in a closed loop and loses its heat to a secondary fluid of the process, such as vapour absorption chillers. The mass flow rate through the solar field and individual CPC tube is governed by requirement of this process, arrangement of the solar field

(series or parallel layout), CPC length and the solar intensity. Unlike flat plate solar water heaters, there is no standard mass flux for testing CPC collectors. For CPC solar water heaters, the water flow rate per unit collector area was varied in the range of 0.02–0.18 kg/s m^2 (Jadhav et al., 2013; Nkwetta et al., 2013; Santos-González et al., 2012). Hsieh (1981) chose a flow rate of 0.063 kg/s m^2 of 80% ethylene glycol mixture, Li et al. (2013) chose heat transfer oil (Therminol 55) flow rates of 0.033 and 0.066 kg/s m^2 while Kim et al. (2013) chose heat transfer oil (Duratherm 600) flow rate between 0.02 and 0.04 kg/s m^2. In the present study, thermal performance at flow rates of up to 0.2 kg/s m^2 has been studied. The atmospheric condition and solar intensity chosen for the study are listed in Table 3.

In this following section, thermal performance of the reference receiver with Therminol 66 as the circulating fluid are discussed. This is followed by presentation and discussion of simulation results for the hybrid receiver with the same perimeter.

5.1. Reference receiver

The variation of receiver surface temperature for the reference design collector with a receiver perimeter of 100 mm and a mass flow rate of 0.01 kg/s, which gives a mass flux in the range of 0.016–0.054 kg/s m^2 of aperture area over a concentration ratio range of 1.2–2.0, is shown in Fig. 6.

Table 3
Ambient condition and solar radiation.

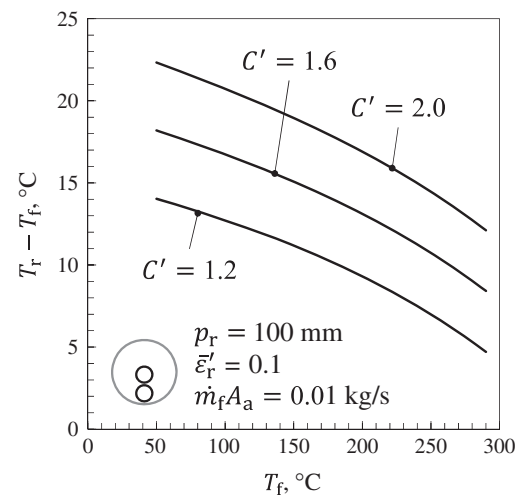| Quantity	Value
Ambient temperature, T_∞	25 °C
Wind heat transfer coefficient, h_{wind}	10 W/m^2 K
Beam radiation intensity on the aperture, I_b	800 W/m^2
Diffuse radiation intensity on the aperture, I_d	200 W/m^2

Fig. 6. Variation in difference of receiver and fluid temperatures with fluid temperature for a 100 mm perimeter U-tube receiver without fins for various geometric concentration ratios.

The receiver emissivity is taken to be 0.1. The receiver temperature above the fluid temperature $(T_r - T_f)$ at any fluid temperature depends on the concentration ratio because the thermal resistance between the receiver and the working fluid is significant. This will result in a collector efficiency factor of less than one. The thermal resistance can be reduced by increasing the mass flow rate through the collector, which leads to a reduction in receiver temperature (see Fig. 7a), reduction in the thermal losses and improvement thermal efficiency (see Fig. 7b). The sharpest drop in receiver temperature happens for mass flux below 0.2 kg/s m^2 where the laminar–turbulent transitional regime occurs. Also with further increase in mass flux, the receiver temperature approaches the fluid temperature so the enhancement in thermal performance is negligible. More importantly, beyond a certain mass flow rate, the effective thermal efficiency reduces due to larger pumping loss. Overall, for low concentration collectors like CPCs, thermal efficiency can be increased by up to 2% by choosing the optimum mass flow rate. The effective thermal efficiency improvement is smaller when the receiver emissivity is low. However, when the mass flow rate through a collector is below 0.2 kg/s m^2, the hybridisation suggested in the present study can be employed to reduce the receiver thermal resistance and thereby improve thermal efficiency. However, in the case of the hybrid receiver, the gap and thermal losses depend on the receiver shape and size, and the overall performance gain needs to be evaluated.

5.2. Hybrid receiver

To compare the performance of a hybrid receiver with the reference receiver, the receiver perimeter is kept constant. For a 100 mm perimeter receiver, at a fixed geometric concentration ratio $C' = 1.2$, fin thickness $\delta = 0.1$ mm, mass flux $\dot{m}_f = 0.052$ kg/s m^2 and fluid temperature $T_f = 200$ °C, the variation of optical, thermal efficiency and effective thermal efficiency due to hybridisation is shown in Fig. 8a. It can be seen that the optical efficiency

Fig. 8. Effect of reducing the tube diameter in a hybrid receiver of 100 mm perimeter with 0.1 mm thick fin on (a) collector performance, and (b) gap loss for beam radiation and view factor from the aperture to the receiver for the diffuse radiation that are given by F_r and F_{ar}, respectively. The optical efficiency for 80:20 proportions of the beam and the diffuse radiation is also shown.

does not show the same trend as F_r because the solar radiation in the present study has a 20% diffuse component whose fraction that reaches the receiver F_{ar} has a very
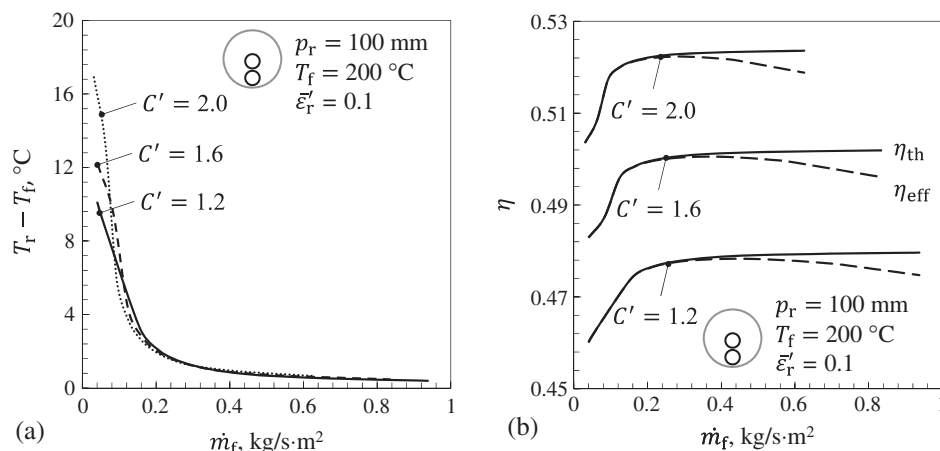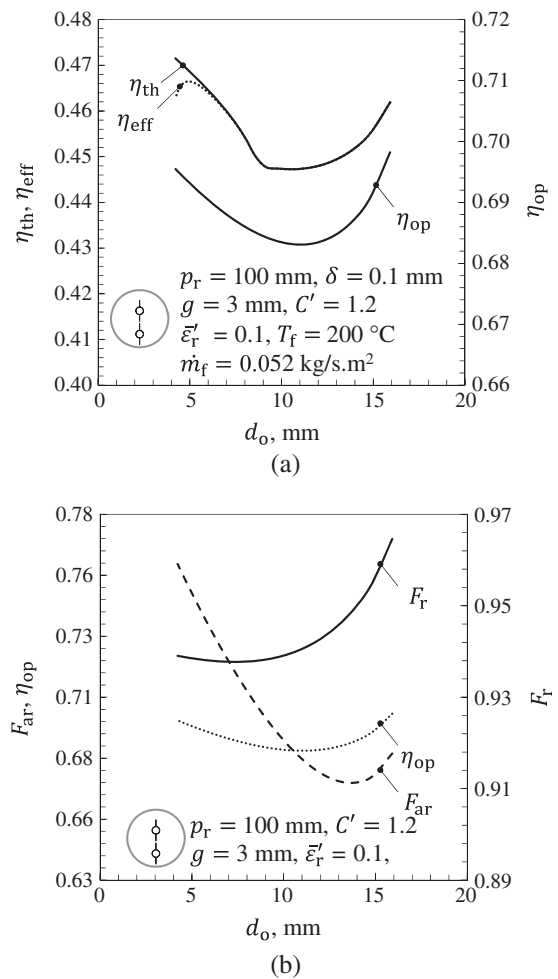

Fig. 7. Effect of mass flux on (a) the difference between the receiver and fluid temperatures, and (b) efficiency of collector for various concentration ratios.

different trend than F_r (see Fig. 8b). Overall, the optical efficiency first decreases with decrease in tube diameter but then starts to increase again. This change in the optical efficiency results in the thermal efficiency following more or less the same trend, but with a slight improvement in the thermal performance at the lowest outside tube diameter of about 3.5 mm (inside tube diameter of 1.5 mm) as compared to the reference receiver. However, the little gain in thermal efficiency comes at the expense of increased pumping power and the effective thermal efficiency improvement is negligible. Furthermore, for this size of the receiver, the thermal resistance of the fins is very small and the thermal performance does not improve much with the increase in fin thickness (see Fig. 9). For the receiver of this size, the variation of thermal performance with the receiver shape is dominated by the gap loss dependent optical efficiency, and thus no performance improvement can be achieved by receiver shape optimization. Lossless CPC can be designed using the cavity/groove method developed by Winston (1980) while allowing for a physical gap between the receiver and the reflector. This method maintains the highest transmission but the leads to reduction in concentration. In such a case, possible improvement in collector efficiency may be achieved by receiver shape optimization.

For larger receivers with lower gap losses, the hybrid receiver can significantly affect the thermal efficiency, as shown in Fig. 10 for a 200 mm perimeter receiver. As compared to the 100 mm perimeter receiver, the gap losses are smaller for this receiver (refer to Fig. 3) and the reduction in heat loss overshadows the marginal increase in gap loss as the tube diameter is reduced. The fins for the 200 mm are longer as compared to the 100 mm receiver, and the thermal resistance of the fin should be minimized by making them thicker to achieve the highest collector performance. However, increasing the fin thickness beyond 0.6 mm does not result in any appreciable performance improvement.

Fig. 10. Effect of reducing the tube diameter in a hybrid receiver of 200 mm perimeter at a thermal oil temperature of 200 °C with fin thickness in the range of 0.1–0.9 mm on the thermal and effective thermal efficiencies.

By appropriately selecting the receiver tube and fin dimensions, the effective thermal performance of a collector with larger receiver can be improved by up to 3%, with the performance gain being higher at lower collector mass flux.

Similar effect of reducing the tube diameter was seen at higher temperature for the large receiver, though the performance improvement, as shown in Fig. 11, is not monotonous with temperature. As the fluid viscosity reduces with increased fluid temperature, laminar–turbulent transition at any flow rate occurs in a comparatively bigger diameter tube (see Fig. 12). With further reduction in tube diameter, the flow gradually becomes fully turbulent. The increase in heat transfer coefficient with Reynolds number is higher in the transition regime as compared to turbulent regime. In the concentrated solar flux of interest in this study, sufficiently low thermal resistance is achieved in the transition regime and further reduction in thermal resistance does not lead to any significant gain in thermal performance. Resultantly the thermal performance improvement is slightly lower at 250 °C as compared to that at 200 °C. Additionally, the increase is pumping power penalty is smaller in the transition regime as compared to turbulent regime. Therefore highest improvement in thermal performance with comparatively small increase in pumping power is achieved in the transition regime. Overall, the effective thermal efficiency improves due to receiver shape optimization, except at 100 °C. At 100 °C the fluid is very viscous and the laminar to turbulent transition happens in very small diameter tubes; the flow velocity is very high in these tubes and the resulting pressure drop is very significant. Resultantly the net performance gain is nearly negligible. In most cases, slightly pressurized water is the preferred collector fluid for a temperature of 150 ° C (saturation pressure of 4.75 bar at 150 °C) as it has higher thermal conductivity and lower viscosity as compared to thermal oils.
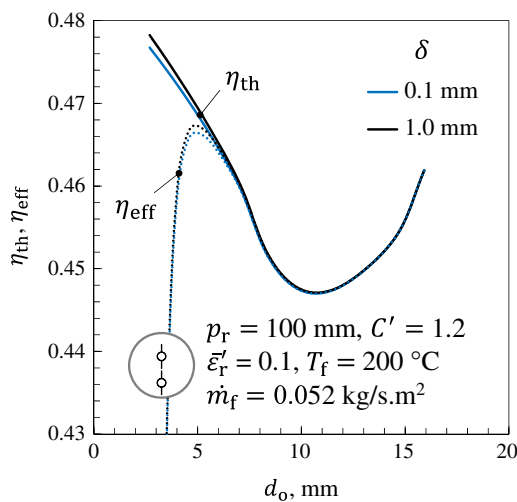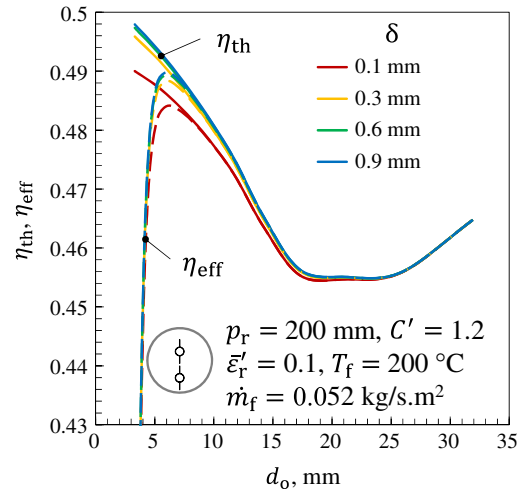

Fig. 9. Comparison of the effect of reducing the tube diameter in a hybrid receiver of 100 mm perimeter at a thermal oil temperature of 200 °C with fin thicknesses of 0.1 and 1 mm on the thermal and effective thermal efficiencies.
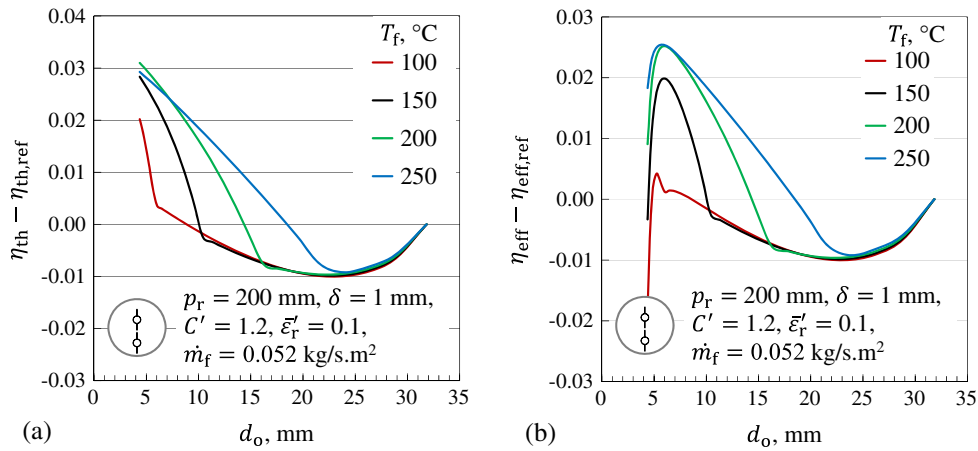
Fig. 11. Effect of reducing the tube diameter in a hybrid receiver of 200 mm perimeter with fin thickness of 1 mm at various thermal oil temperatures on the (a) thermal efficiency and (b) effective thermal efficiencies.
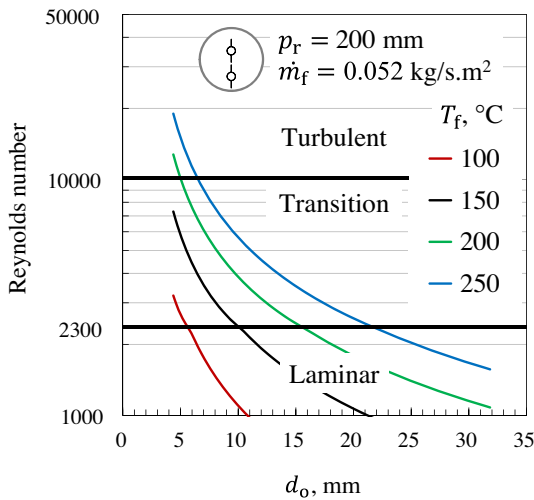

Fig. 12. Variation in flow Reynolds number with reduction in receiver tube diameter of a 200 mm perimeter receiver for different thermal oil temperatures at a fixed mass flux of 0.052 kg/s m^2. The various flow regimes have been marked.

Comparison of the effect of concentration ratio on collector thermal performance of the hybrid collector with a thick fin of 1 mm is shown in Fig. 13, where it can be seen that the performance improvement can be achieved at all concentration ratios. For the same receiver area and mass flux, the mass flow rate through the receiver increases with concentration ratio and laminar to turbulent transition happens in bigger diameter tubes. Resultantly, the performance enhancement decreases with increase in concentration ratio. Similarly performance enhancement can be seen at low to moderate flow rate but no performance enhancement is seen at a mass flux of 0.2 kg/s m^2 as the improvement in thermal efficiency is small but the pumping power penalty is high (see Fig. 14). The improvement in thermal efficiency with receiver shape optimization is slightly higher for a higher emissivity receiver as shown in Fig. 15.

Simulations were also performed with water as the working fluid at temperatures up to 150 °C and using temperature dependent thermophysical properties calculated at
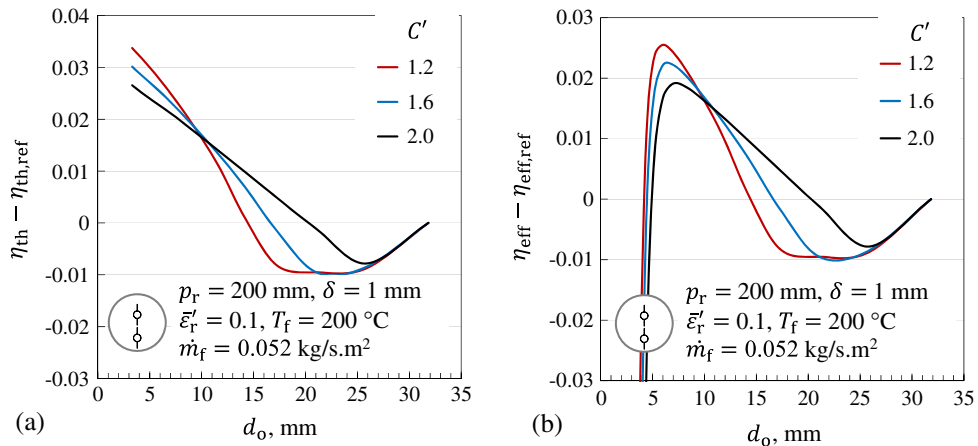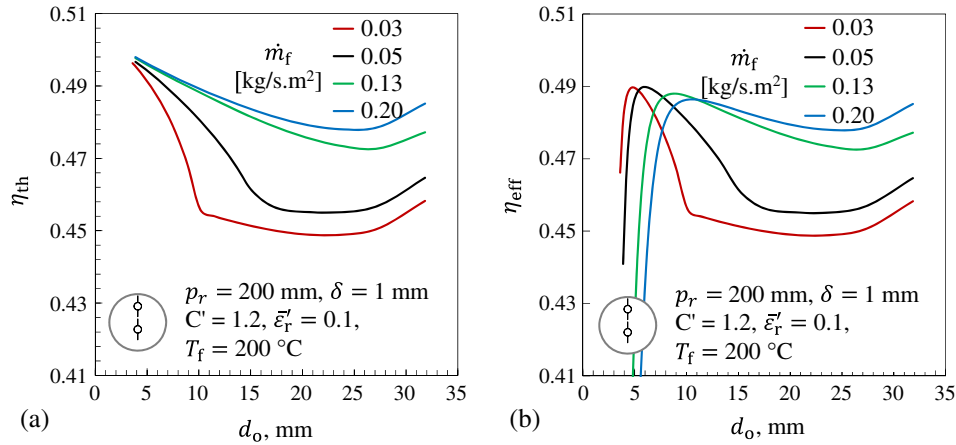

Fig. 13. Effect of reducing the tube diameter in a hybrid receiver of 200 mm perimeter with fin thickness of 1 mm at a thermal oil temperature of 200 °C and different geometric concentration ratios on the (a) thermal efficiency and (b) effective thermal efficiencies. The subscript "ref" indicates the U-tube receiver without fins.

Fig. 14. Effect of reducing the tube diameter in a hybrid receiver of 200 mm perimeter with fin thickness of 1 mm at a thermal oil temperature of 200 °C and different mass flux on the (a) thermal efficiency and (b) effective thermal efficiencies.
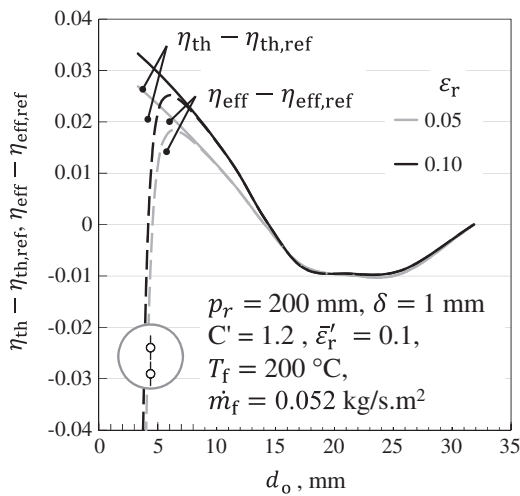

Fig. 15. Effect of reducing the tube diameter in a hybrid receiver of 200 mm perimeter with fin thickness of 1 mm at a thermal oil temperature of 200 °C and different receiver emissivities on the thermal and effective thermal efficiencies. The subscript "ref" indicates the reference receiver (U-tube receiver without fins).

the film temperature. Both with water and thermal oil as the working fluid, no effective performance improvement is achieved by the reduction of tube diameter at a mean fluid temperature of 100 °C (see Fig. 16). However, the thermal resistance of water is much lower than thermal oil at this temperature as water has higher thermal conductivity and lower viscosity (transition regime happens even for the largest tube) and overall collector efficiency is higher. Water is therefore a recommended working fluid for temperatures up to 150 °C. In general, the performance improvement by reducing the tube diameter with water over a wide range of mass flow rate and temperature up to 150 °C is marginal (see Fig. 17).

The results of this study show that there is a scope for the optimization of the collector shape specifically at low to moderate thermal oil flow rates typically expected in CPC collectors and fluid temperature above 150 °C. For a mass flow rate of less than 0.15 kg/s m^2, the optimum performance is achieved when the flow is in transition-turbulent regime and the tube diameter is always between 5 and 10 mm.
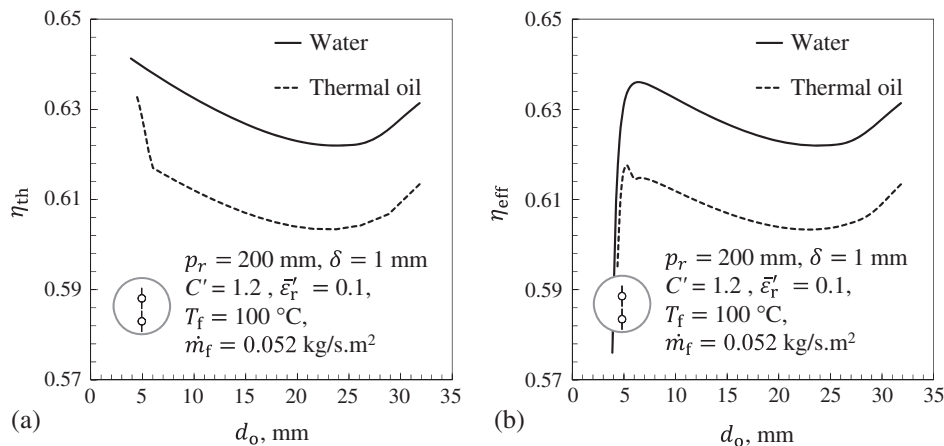

Fig. 16. Comparison of the effect of reducing the tube diameter in a hybrid receiver of 200 mm perimeter with fin thickness of 1 mm at a fluid temperature of 200 °C with water and thermal oil as the fluids on the (a) thermal efficiency and (b) effective thermal efficiencies.
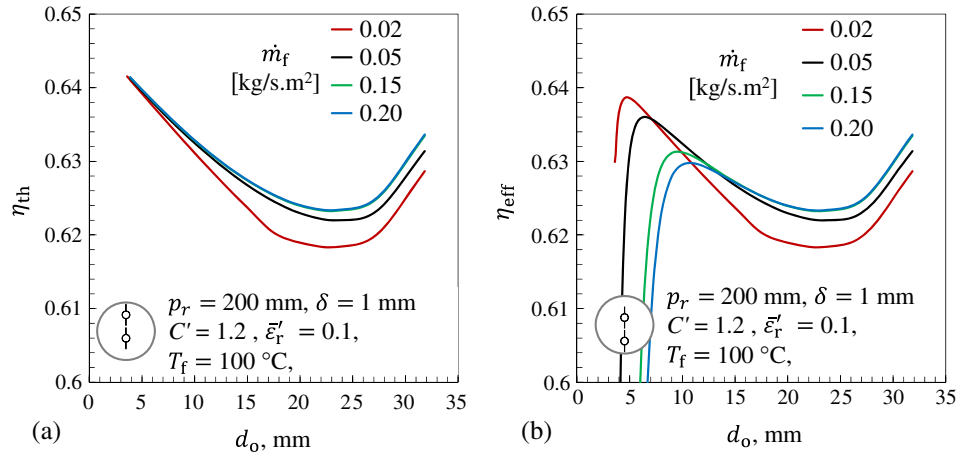
Fig. 17. Effect of reducing the tube diameter in a hybrid receiver of 200 mm perimeter with fin thickness of 1 mm at a water temperature of 100 °C and different mass flux on the (a) thermal efficiency and (b) effective thermal efficiencies. The subscript "ref" indicates the reference receiver (U-tube receiver without fins).

6. Conclusions

In this paper the thermohydraulic performance of a bifacially irradiated receiver which is a hybrid of a flat and U-tube receiver in a vacuum enclosure with a compound parabolic concentrator and collector fluid (Therminol 66) temperature in the range of 100–300 °C is modelled. Effective thermal efficiency of the collector can be maximized by optimizing the receiver shape (tube and fin dimensions). The optimum shape depends on the receiver area, gap size, concentration ratio, mass flux, fluid temperature, selective surface emissivity, etc. Generally, highest effective thermal efficiency is achieved in the laminar–turbulent transitional Reynolds number regime. At low temperatures of 100 °C, laminar–turbulent transitional regime may not be achievable by reducing the flow passages without significantly increasing pumping power, so the thermal and the effective thermal efficiency cannot be improved by constraining the flow passage. Indeed slightly pressurized water should be the preferred collector fluid for a temperature of 150 °C (saturation pressure of 4.75 bar at 150 °C) as it has higher thermal conductivity and lower viscosity as compared to thermal oils. For small receivers, the receiver–reflector gap results in a decrease in optical efficiency as the tube diameter is reduced and the effective thermal efficiency gain is insignificant. In most of the other cases where the receiver perimeter is large, flow rate is low to moderate (less than 0.15 kg/s m^2) and the fluid is not very viscous, the effective thermal efficiency can be improved by appropriately selecting tube diameter using the presented thermal model. For a mass flux of less than 0.15 kg/s m^2, the optimum outer tube diameter (tube wall thickness is 1 mm) is always between 5 and 10 mm and depending on the receiver perimeter, the optimum fin thickness (made of copper) can be up to 1 mm. For water at temperature up to 150 °C as collector fluid, the performance enhancement by receiver shape optimization

is marginal. However, the collector performance with water as the working fluid is superior as compared to thermal oil at these temperatures. These results of this study show that there is a scope for the optimization of the collector shape in CPC collectors for medium to high temperature applications.

Appendix A. View factors

Determining the view factor between the aperture and the receiver is complex as the aperture does not enclose the receiver and the CPC mirrors are concave. To determine it, a very detailed ray tracing study needs to be performed, which is out of the scope of this study. To simplify the analysis, we assume that all the radiation that originates from the virtual receiver enclosing the receiver "v" can reach the aperture either directly or with the help of the CPC reflectors after several reflections (Rabl, 1976), i.e. the view factor from the virtual receiver "v" to the aperture is

$$F_{va} = 1. \tag{A.1}$$

The view factor from the virtual receiver "v" to the receiver is

$$F_{vr} = 1. \tag{A.2}$$

From reciprocity relation we know that $A_r F_{rv} = A_v F_{vr}$. Therefore, F_{rv} is given as

$$F_{rv} = A_v / A_r. \tag{A.3}$$

The view factor from the receiver to the aperture can be derived as

$$F_{ra} = F_{rv} \times F_{va} = A_v/A_r. \tag{A.4}$$

Again applying the reciprocity rule between the aperture and the receiver, and combining with Eq. (A.5) yields

$$F_{ar} = F_{ra} \times A_r/A_a = A_v/A_a. \tag{A.5}$$

Similar to F_{va}, F_{ea} is assumed to be 1. As the aperture and the enclosure are of similar area, F_{ae} is also assumed to be 1. As the enclosure completely surrounds the virtual receiver enclosing the receiver, and the virtual receiver is not concave, $F_{ve} = 1$. The view factor from the receiver to the enclosure is therefore given by

$$F_{re} = F_{rv} \times F_{ve} = A_v/A_r. \tag{A.6}$$

Again applying the reciprocity rule between the aperture and the receiver, and combining with Eq. (A.7) yields

$$F_{er} = F_{re} \times A_r/A_e = A_v/A_e. \tag{A.7}$$

Appendix B. Virtual receiver's perimeter

The area of the virtual receiver surrounding the receiver "v" is shown in Fig. B.1(a) and is given by

$$
\begin{aligned}
A_v &= \overline{\text{ABCDE}'\text{F}'\text{G}'\text{HIJA}} \times l \\
&= \left(\overline{\text{AB}} + \overline{\text{BC}} + \overline{\text{CD}} + \overline{\text{DE}'} + \overline{\text{E}'\text{F}'} + \overline{\text{F}'\text{G}'} \right. \\
&\quad \left. + \overline{\text{G}'\text{H}} + \overline{\text{HI}} + \overline{\text{IJ}} + \overline{\text{JA}} \right) \times l,
\end{aligned} \tag{B.1}
$$

where

$$\overline{\text{AB}} = \overline{\text{E}'\text{F}'} = \overline{\text{F}'\text{G}'} = \overline{\text{JA}} = \sqrt{w^2 + wd_0}, \tag{B.2}$$

$$\overline{\text{BC}} = \overline{\text{DE}'} = \overline{\text{JI}} = \overline{\text{G}'\text{H}} = d_0 \left[\frac{\pi}{4} - \frac{1}{2} \arccos \left(\frac{d_0}{d_0 + 2w} \right) \right], \tag{B.3}$$

and

$$\overline{\text{CD}} = \overline{\text{HI}} = 2w + d_0. \tag{B.4}$$

Substituting the segment lengths from Eqs. (B.2)–(B.4) in Eq. (B.1) gives

$$A_v = 4l\sqrt{w^2 + wd_0} + 4wl + d_0l \left[2 + \pi - 2\arccos \left(\frac{d_0}{d_0 + 2w} \right) \right]. \tag{B.5}$$

The area of the virtual receiver surrounding the receiver and the gap "V" is shown in Fig. B.1(b) and is given by

$$
\begin{aligned}
A_V &= \overline{\text{ABCDEFGHIJA}} \times l \\
&= \left(\overline{\text{AB}} + \overline{\text{BC}} + \overline{\text{CD}} + \overline{\text{DE}} + \overline{\text{EF}} + \overline{\text{FG}} \right. \\
&\quad \left. + \overline{\text{GH}} + \overline{\text{HI}} + \overline{\text{IJ}} + \overline{\text{JA}} \right) \times l,
\end{aligned} \tag{B.6}
$$

where

$$\overline{\text{DE}} = \overline{\text{GH}} = d_0 \left[\frac{\pi}{4} - \frac{1}{2} \arccos \left(\frac{d_0}{d_0 + 2w + 2g} \right) \right], \tag{B.7}$$

and

$$\overline{\text{EF}} = \overline{\text{FG}} = \sqrt{(w + g)^2 + (w + g)d_0}. \tag{B.8}$$

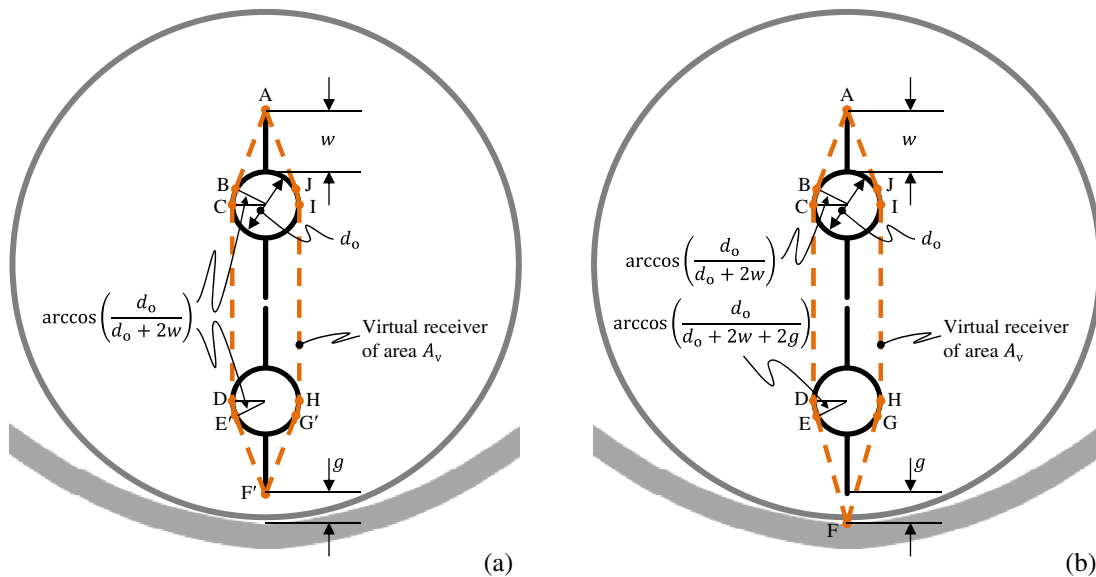Substituting the segment lengths from Eqs. (B.2)–(B.4), (B.7) and (B.8) in Eq. (B.6) gives

Fig. B.1. Schematics showing the sections that make (a) the virtual receivers enclosing the receiver and (b) the virtual receiver enclosing the receiver and the gap.

$$A_V = 2l\sqrt{w^2 + wd_o} + 2l\sqrt{(w+g)^2 + (w+g)d_o} + 4wl$$
$$+ d_o l \left[2 + \pi - \arccos\left(\frac{d_o}{d_o + 2w}\right) \right.$$
$$\left. - \arccos\left(\frac{d_o}{d_o + 2w + 2g}\right) \right]. \qquad (B.9)$$

References

Australian/New Zealand Standard, 2007. Test Methods for Solar Collectors Part 1: Thermal Performance of Glazed Liquid Heating Collectors Including Pressure Drop (ISO 9806-1:1994, MOD).

Balkoski, K.M., 2011. Performance Analysis of Medium Temperature Non-Tracking Solar Thermal Concentrators, MSc Thesis. University of California Merced.

Bliss Jr., R.W., 1959. The derivations of several "Plate-efficiency factors" useful in the design of flat-plate solar heat collectors. Sol Energy 3 (4), 55–64. http://dx.doi.org/10.1016/0038-092X(59)90006-4.

Cheng, N., 2008. Formulas for friction factor in transitional regimes. J. Hydraulic Eng. 134 (9), 1357–1362. http://dx.doi.org/10.1061/(ASCE)0733-9429(2008)134:9(1357).

Duffie, J.A., Beckman, W.A., 2013. Solar Engineering of Thermal Processes, fourth ed. John Wiley & Sons Inc., USA. http://dx.doi.org/10.1002/9781118671603.

Gajic, M., Karwa, N., Mojiri, A., Rosengarten, G., 2014. Reflection losses from an evacuated tube in a CPC. In: Light, Energy and the Environment: Optics for Solar Energy, Canberra, Australia. Optical Society of America. RTu2B.6. http://dx.doi.org/10.1364/OSE.2014.RTu2B.6.

Gajic, M., Karwa, N., Mojiri, A., Rosengarten, G., 2015. Modeling reflection loss from an evacuated tube inside a compound parabolic concentrator with a cylindrical receiver. Optics Express 23 (11), A493–A501. http://dx.doi.org/10.1364/oe.23.00a493.

Gnielinski, V., 2010. G1 heat transfer in pipe flow. VDI Heat Atlas. Springer, Berlin, Heidelberg, pp. 691–700. http://dx.doi.org/10.1007/978-3-540-77877-6_34.

Hall, S., 2012. Branan's Rules of Thumb for Chemical Engineers, fifth ed. Butterworth-Heinemann, Waltham, MA, <http://www.sciencedirect.com/science/book/9780123877857>.

Ho, C.D., Chen, T.C., 2008. Collector efficiency improvement of recyclic double-pass sheet-and-tube solar water heaters with internal fins attached. Renew. Energy 33 (4), 655–664. http://dx.doi.org/10.1016/j.renene.2007.04.002.

Hong, S.W., Bergles, A.E., 1976. Augmentation of laminar flow heat transfer in tubes by means of twisted-tape inserts. J Heat Trans. 98 (2), 251. http://dx.doi.org/10.1115/1.3450527.

Hsieh, C.K., 1981. Thermal analysis of CPC collectors. Sol Energy 27 (1), 19–29. http://dx.doi.org/10.1016/0038-092X(81)90016-5.

Institut für Solartechnik, 2009. Qualification Test of Solar Absorber Coating Durability. Document Number: SKN_N0115R0. <http://www.estif.org/solarkeymark/Links/Internal_links/network/sknwebdoclist/SKN_N0115R0.pdf>.

Institut für Solartechnik, 2013. Prüfprotokoll: Reflexion. Document Number: ALMA1304000Z. <http://www.almecogroup.com/uploads/1127-tinox_energy_al_spektrum.pdf>.

Jadhav, A.S., Gudekar, A.S., Patil, R.G., Kale, D.M., Panse, S.V., Joshi, J.B., 2013. Performance analysis of a novel and cost effective CPC system. Energy Convers. Manage. 66, 56–65. http://dx.doi.org/10.1016/j.enconman.2012.09.030.

Jaisankar, S., Radhakrishnan, T.K., Sheeba, K.N., 2009. Experimental studies on heat transfer and friction factor characteristics of forced circulation solar water heater system fitted with helical twisted tapes. Sol Energy 83 (11), 1943–1952. http://dx.doi.org/10.1016/j.solener.2009.07.006.

Karwa, R., Solanki, S.C., Saini, J.S., 2001. Thermo-hydraulic performance of solar air heaters having integral chamfered rib roughness on

absorber plates. Energy 26 (2), 161–176. http://dx.doi.org/10.1016/S0360-5442(00)00062-1.

Kim, Y.S., Balkoski, K., Jiang, L., Winston, R., 2013. Efficient stationary solar thermal collector systems operating at a medium-temperature range. Appl. Energy 111, 1071–1079. http://dx.doi.org/10.1016/j.apenergy.2013.06.051.

Li, X., Dai, Y.J., Li, Y., Wang, R.Z., 2013. Comparative study on two novel intermediate temperature CPC solar collectors with the U-shape evacuated tubular absorber. Sol Energy 93, 220–234. http://dx.doi.org/10.1016/j.solener.2013.04.002.

Li, Z., Ye, X., Liu, J., 2014a. Optimal temperature of collector for solar double effect LiBr/H$_2$O absorption cooling system in subtropical city based on a year round meteorological data. Appl. Therm. Eng. 69 (1–2), 19–28. http://dx.doi.org/10.1016/j.applthermaleng.2014.04.039.

Li, Z., Ye, X., Liu, J., 2014b. Performance analysis of solar air cooled double effect LiBr/H$_2$O absorption cooling system in subtropical city. Energy Convers. Manage. 85, 302–312. http://dx.doi.org/10.1016/j.enconman.2014.05.095.

Nkwetta, D.N., Smyth, M., Haghighat, F., Zacharopoulos, A., Hyde, T., 2013. Experimental performance evaluation and comparative analyses of heat pipe and direct flow augmented solar collectors. Appl. Therm. Eng. 60 (1-2), 225–233. http://dx.doi.org/10.1016/j.applthermaleng.2013.06.059.

O'Gallagher, J.J., 2008. Nonimaging optics in solar energy. Synth. Lect. Energy Environ.: Technol. Sci. Soc. 2 (1), 1–120. http://dx.doi.org/10.2200/S00120ED1V01Y200807EGY002.

Rabl, A., 1976. Comparison of solar concentrators. Sol Energy 18 (2), 93–111. http://dx.doi.org/10.1016/0038-092X(76)90043-8.

Rabl, A., Goodman, N.B., Winston, R., 1979. Practical design considerations for CPC solar collectors. Sol Energy 22 (4), 373–381. http://dx.doi.org/10.1016/0038-092X(79)90192-0.

Robles, A., Duong, V., Martin, A.J., Guadarrama, J.L., Diaz, G., 2014. Aluminum minichannel solar water heater performance under year-round weather conditions. Sol Energy 110, 356–364. http://dx.doi.org/10.1016/j.solener.2014.09.031.

Santos-González, I., Ortega, N., Gómez, V.H., García-Valladares, O., Best, R., 2012. Development and experimental investigation of a compound parabolic concentrator. Int. J. Energy Res. 36 (12), 1151–1160. http://dx.doi.org/10.1002/er.1866.

SCHOTT Technical Glass Solutions GmbH, 2009. BOROFLOAT 33 – Optical Properties. <http://www.schott.com/borofloat/english/download/borofloat33_opt_en_web.pdf>.

Sharma, N., Diaz, G., 2011. Performance model of a novel evacuated-tube solar collector based on minichannels. Sol Energy 85 (5), 881–890. http://dx.doi.org/10.1016/j.solener.2011.02.001.

Solutia Inc., 2001. Therminol 66. <http://twt.mpei.ac.ru/TTHB/HEDH/HTF-66.pdf>.

Trudeau, N., Francoeur, M., 2008. Energy Efficiency Indicators for Public Electricity Production from Fossil Fuels, IEA. <http://www.iea.org/>.

US State Electricity Profiles. US Energy Information Administration. <http://www.eia.gov/electricity/state/> (retrieved July 15, 2015).

Winston, R., 1978. Ideal flux concentrators with reflector gaps. Appl. Opt. 17 (11), 1668–1669. http://dx.doi.org/10.1364/AO.17.001668.

Winston, R., 1980. Cavity enhancement by controlled directional scattering. Appl. Opt. 19 (2), 195–197. http://dx.doi.org/10.1364/AO.19.000195.

Winston, R., 2012. Design and Development of Low-Cost, High-Temperature Solar Collector For Mass Production, California Energy Commission. Publication Number: CEC-500-2012-050,.

Winston, R., Jiang, L., Widyolar, B., 2014. Performance of a 23 KW solar thermal cooling system employing a double effect absorption chiller and thermodynamically efficient non-tracking concentrators. Energy Procedia. 48, 1036–1046. http://dx.doi.org/10.1016/j.egypro.2014.02.118.

Yeh, H.M., Ho, C.D., Yeh, C.W., 2003. Effect of aspect ratio on the collector efficiency of sheet-and-tube solar water heaters with the consideration of hydraulic dissipated energy. Renew. Energy. 28 (10), 1575–1586. http://dx.doi.org/10.1016/s0960-1481(03)00006-5.